Tightly Bound Excitons in Monolayer WSe_2

Keliang He,[1] Nardeep Kumar,[2] Liang Zhao,[1] Zefang Wang,[1] Kin Fai Mak,[3] Hui Zhao,[2] and Jie Shan[1]
[1]*Department of Physics, Case Western Reserve University, 10900 Euclid Avenue, Cleveland, Ohio 44106, USA*
[2]*Department of Physics and Astronomy, The University of Kansas, Lawrence, Kansas 66045, USA*
[3]*Kavli Institute at Cornell for Nanoscale Science and Laboratory of Atomic and Solid State Physics, Cornell University, Ithaca, New York 14853, USA*

(Received 12 February 2014; revised manuscript received 16 April 2014; published 10 July 2014)

Exciton binding energy and excited states in monolayers of tungsten diselenide (WSe_2) are investigated using the combined linear absorption and two-photon photoluminescence excitation spectroscopy. The exciton binding energy is determined to be 0.37 eV, which is about an order of magnitude larger than that in III–V semiconductor quantum wells and renders the exciton excited states observable even at room temperature. The exciton excitation spectrum with both experimentally determined one- and two-photon active states is distinct from the simple two-dimensional (2D) hydrogenic model. This result reveals significantly reduced and nonlocal dielectric screening of Coulomb interactions in 2D semiconductors. The observed large exciton binding energy will also have a significant impact on next-generation photonics and optoelectronics applications based on 2D atomic crystals.

DOI: 10.1103/PhysRevLett.113.026803 PACS numbers: 73.21.Fg, 71.35.Cc, 78.20.Ci, 78.55.Hx

One of the most distinctive features of electrons in two-dimensional (2D) semiconductors, such as single atomic layers of group VI transition metal dichalcogenides (TMDs) [1], is the significantly reduced dielectric screening of Coulomb interactions. An important consequence of strong Coulomb interactions is the formation of tightly bound excitons. Indeed, recent theoretical studies have predicted a large exciton binding energy between 0.5 and 1 eV in MoS_2 monolayers [2–10], a representative 2D direct gap semiconductor from the family of TMDs [11,12]. These values for the exciton binding energy are more than an order of magnitude larger than that in conventional III-V-based quasi-2D semiconductor quantum wells (QWs) [13,14]. Such tightly bound excitons are expected to not only dominate the optical response, but also to play a defining role in the optoelectronic processes, such as photoconduction and photocurrent generation in 2D semiconductors [1,15]. On the other hand, little is known about these tightly bound excitons from the experimental standpoint, except the energy of the lowest energy one-photon active exciton states [11] and an indirect evidence of large binding energies through recent studies on trions, quasiparticles of two electrons and a hole, or two holes and an electron [16–18]. Furthermore, a non-Rydberg series has been predicted for excitons in 2D semiconductors, arisen from the nonlocal character of screening of the Coulomb interactions [4,19]. While a Rydberg series for the exciton energy spectrum has been observed in *bulk* MoS_2 [20,21], similar experimental studies on monolayers of MoS_2 or other TMDs have not been reported [22].

The challenge in experimental determination of the exciton binding energy in 2D TMDs by linear optical methods, commonly used for bulk semiconductors [23] or conventional semiconductor QWs [13], lies in the identification of the onset of band-to-band transitions in the optical absorption or emission spectrum. Such an onset of band-to-band transitions has not been observed in 2D TMDs presumably due to the significant transfer of oscillator strengths from the band-to-band transitions to the fundamental exciton states, lifetime broadening, and potential overlap in energy with exciton states originated from higher energy bands and/or different parts of the Brillouin zone [11]. An alternative is to determine the exciton excited states and evaluate the binding energy from the level spacing based on a model. In the simple 2D hydrogenic model [24], where an electron-hole (e–h) pair in 2D interacts through a Coulomb potential, the energy spectrum is known as the Rydberg series $E_n = -[E_b/(n-1/2)^2]$ with an exciton binding energy $4E_b$. Each state $n(=1,2,3\ldots)$ is degenerate with angular momentum $l = 0, \pm 1, \ldots, \pm(n-1)$. For instance, the $2s$ ($l = 0$, one-photon allowed) and $2p$ ($l = \pm 1$, two-photon allowed) states are degenerate, lying at $8/9$ of the exciton binding energy above the lowest energy $1s$ state. Measurements of the $1s$ and $2s/2p$ states allow the determination of the exciton binding energy in the 2D hydrogenic model.

In this Letter, we report a combined linear and nonlinear optical study on the exciton excited states and binding energy in monolayers of WSe_2, a 2D direct gap semiconductor from the family of TMDs, with optical and electronic properties similar to MoS_2. Our linear absorption measurement reveals up to five s states from the A exciton series even at room temperature. Two-photon photoluminescence (2PPL) excitation spectroscopy [25–27] is employed to probe the p states and measure the band

edge energy directly. A band gap energy of 2.02 eV and an exciton binding energy of 0.37 eV have been determined for monolayer WSe_2 from the experimental results without relying on any specific exciton models. Further, the measured exciton excitation spectrum with much more evenly spaced energy levels is very distinct from the simple 2D hydrogenic model. This behavior can be qualitatively understood as a consequence of the nonlocal character of dielectric screening in 2D [4,19]. Our experiment thus directly verifies the importance of Coulomb interactions and excitonic effects in 2D semiconductors. The unique spectrum of exciton states with differing optical activities revealed by our experiment also presents new opportunities for the study and control of the spin/valley polarization in 2D TMDs through interexcitonic and intraexcitonic processes [28–33].

In our experiment, atomically thin WSe_2 samples were mechanically exfoliated from their bulk form (2D semiconductors) onto Si substrates covered with a 100- or 300-nm SiO_2 layer or fused quartz substrates. Monolayer samples were first identified according to their optical contrast with the substrate [Fig. 1(a)] and then confirmed by photoluminescence (PL) spectroscopy [Fig. 1(b)]. The PL was excited with a continuous wave (cw) HeNe laser at 1.96 eV and recorded with a grating spectrometer equipped with either a liquid nitrogen or thermoelectrically cooled

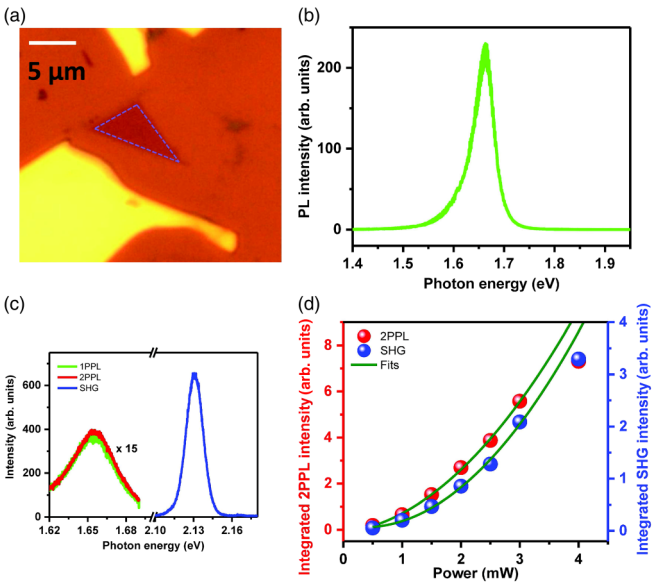

FIG. 1 (color online). (a) Optical reflection image of WSe_2 flakes on a Si substrate covered by a 300-nm SiO_2 layer. A monolayer sample (middle) is outlined by dashed blue lines. (b) PL spectrum of monolayer WSe_2 excited by a cw HeNe laser at 1.96 eV. (c) Emission spectrum of monolayer WSe_2 under the excitation of femtosecond IR pulses centered at 1.07 eV. It consists of two features corresponding to the SHG (blue) and two-photon PL (red). The latter is magnified by 15 times. The PL excited by the cw HeNe laser (green) is included for comparison. (d) Excitation power dependence of the integrated SHG and two-photon PL.

CCD camera. A single narrow peak at ~1.65 eV at room temperature (corresponding to the lowest energy exciton state A) with no lower energy indirect gap emission features confirms the monolayer thickness [34,35].

To probe the one-photon active exciton states, the linear absorption spectrum of monolayer WSe_2 was measured through the reflection contrast using broadband radiation from a supercontinuum laser as described elsewhere [11,36]. In short, the laser beam was focused onto the samples with a ×50 microscope objective to a spot size of ~2 μm. Typically several hundred spectra of reflection contrast were averaged to improve the signal-to-noise ratio. A typical spectral resolution is ~0.3 meV.

To access the two-photon active exciton states in monolayer WSe_2, femtosecond infrared (IR) pulses in the energy range of 0.85 to 1.1 eV generated from an optical parametric oscillator pumped by a Ti:sapphire laser were employed. The IR-excited PL via two-photon absorption, instead of the direct attenuation of the IR excitation beam, was measured for higher detection sensitivity. The IR pulses were ~100 fs in duration with a repetition rate of ~80 MHz. They were focused onto the samples by a × 20 IR objective to a spot size of ~2 μm under normal incidence. The backscattered signal was collected by the same objective and sent to a spectrometer after appropriate filtering. The energy of the IR source was tuned with a step size of ~10 meV to obtain the 2PPL excitation spectrum. The spectral resolution is ~20 meV determined by the bandwidth of the IR excitation pulses. To calibrate the variations in the IR pulse duration and beam size while changing its energy, we simultaneously measure the second-harmonic generation (SHG) from a z-cut single crystal quartz plate as a reference (see below). An excitation power below 2 mW and 100 μW, respectively, has been employed for the nonlinear and linear absorption measurements to avoid heating and radiation damage of the samples. No observable changes for both the PL spectral shape and quantum yield throughout the entire measurement on any sample were observed.

Figure 2(a) illustrates the linear absorption spectrum of monolayer WSe_2 on fused quartz (red line). In the energy range of 1.5–2.3 eV, there are two prominent exciton peaks at 1.65 and 2.08 eV, respectively. These peaks, labeled A and B, correspond to the lowest energy exciton states originated from transitions from the two highest energy spin-orbit split-off valence bands to the lowest energy conduction bands around the $K(K')$ point in the Brillouin zone [34]. The large energy separation between the A and B exciton state (~0.43 eV) due to strong spin-orbit coupling in WSe_2 opens up a window for the observation of exciton excited states of the A series. Below we focus only on the A exciton series.

A careful examination of the linear absorption spectrum reveals resonance A' at 1.82 eV, about 0.16 eV above the prominent A peak. Furthermore, three additional resonances at higher energies with increasingly smaller oscillator strengths (marked with $*$) can be identified as dips from

the second-order numerical derivative of the absorption spectrum [23] [Fig. 2(b)]. These features have been observed in all five samples studied in this experiment. The dip immediately above the A' energy (with an amplitude smaller than the next identified resonance) was not reproduced and likely an artifact. For temperature <150 K, a sixth resonance can also be identified. Further, all of these identified resonance features show a similar blue shift with temperature as the A peak, dictated primarily by temperature renormalization of the band gap [15,23]. (See the Supplemental Material [37], Sec. 2, for details on the experimental results and their analysis.) Based on these evidences, we assign these features as one-photon active states from the A exciton series and label them in order of increasing energy as $1s$, $2s$… in analogy to the hydrogenic Rydberg series. We note that first the large level spacing of $E_{5s} - E_{1s} \sim 0.3$ eV suggests that the exciton binding energy is at least 0.3 eV. Second, we did not observe any noticeable dependence of the states on substrate studied in this experiment. And third, while the $1s$ state narrows from ~40 meV at room temperature to ~10 meV at 30 K [see the Supplemental Material [37], Fig. S(4)], consistent with an earlier PL measurement on the same material [33], the width of the $2s$ and $3s$ states (~30 meV) does not depend on temperature. The latter is a clear evidence of significant lifetime broadening from effects such as energy-dependent exciton-phonon scattering. Given the significant lifetime broadening for the exciton excited states, we focus on room temperature in the nonlinear optical study below.

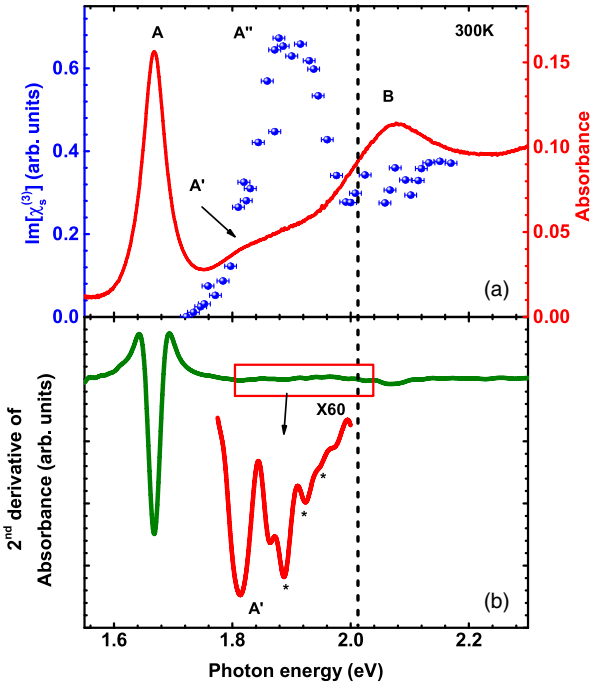

FIG. 2 (color online). (a) Linear absorption (red line, right axis) and 2PPL excitation spectrum (blue symbols, left axis) measured on monolayer WSe_2 at room temperature. Each data point of the 2PPL excitation spectrum corresponds to an integrated PL (1.664–1.687 eV) normalized by the reference SHG signal from a z-cut quartz crystal according to Eq. (1). The uncertainty corresponds to the spectral resolution, determined by the bandwidth of the excitation pulse. A and B correspond to the fundamental exciton resonances arisen from transitions from the two highest energy spin-orbit split-off valance bands and the lowest energy conduction bands at the $K(K')$ point of the Brillouin zone. A' and A'' denote the $2s$ state and a broad p peak observed in one- and two-photon absorption, respectively. (b) Second-order numerical derivative of the linear absorption spectrum of (a). Black dashed line denotes the band edge energy of 2.02 eV determined from the fit described in the text.

Now we turn to the discussion of the two-photon allowed exciton states. In Fig. 1(c), we show the emission spectrum of monolayer WSe_2 in the visible range under excitation of an IR pulse of energy $\hbar\omega = 1.07$ eV. The spectrum consists of a narrow peak at $2\hbar\omega$ (blue line), corresponding to the SHG from monolayer WSe_2 [35], and a weaker feature peaked at 1.65 eV (red line). The latter matches the PL spectrum of the sample under cw excitation (green line) and depends on the excitation power quadratically as the second-harmonic (SH) signal [Fig. 1(d)]. It is thus confirmed that PL can indeed be induced through two-photon absorption and is used to characterize the two-photon absorbance.

Two-photon absorption in a sample can be described as a third-order nonlinear process and the two-photon absorbance, by the imaginary part of the third-order nonlinear susceptibility $\mathrm{Im}[\chi_S^{(3)}(\omega, -\omega, \omega)]$. To extract this parameter, we normalize the 2PPL intensity $I_{2\mathrm{PPL},S}$ from the sample by the SH intensity detected from a reference, $I_{2\omega,Q}$, under identical experimental conditions. z-cut single crystal quartz was chosen as the reference because both the fundamental and SH frequency for the energy range studied here are far away from the quartz band gap, and the dispersion in both the linear and nonlinear optical properties can be ignored [40]. If we assume the PL quantum yield is independent of the IR excitation energy, the third-order nonlinear sheet susceptibility of a monolayer sample on a substrate can be derived as [41]

$$\mathrm{Im}[\chi_S^{(3)}(\omega, -\omega, \omega)] \propto \omega^{-1} |L_\omega^{-4}| \frac{I_{2\mathrm{PPL},S}}{I_{2\omega,Q}}. \qquad (1)$$

Here L_ω is the local field factor at the fundamental frequency, which converts the incident excitation field to the field in the sample, and the factor ω^{-1} arises from processes at the surface or interface. For the experimental geometry of monolayer samples on Si covered with a SiO_2 layer of thickness L_{SiO_2}, the local field factor is given as $L_\omega = t_{12}/(1 - r_{23} r_{21} e^{-2i\varphi})$ with Fresnel coefficients $t_{12} = 2/(1 + n_{SiO_2})$, $r_{21} = (n_{SiO_2} - 1)/(n_{SiO_2} + 1)$, $r_{23} = (n_{SiO_2} - n_{Si})/(n_{SiO_2} + n_{Si})$ and phase shift $\varphi = n_{SiO_2} \omega L_{SiO_2}/c$ from propagation in the SiO_2 layer.

Figure 3(a) illustrates the normalized 2PPL spectra $I_{2\mathrm{PPL},S}/I_{2\omega,Q}$ of a monolayer sample of WSe_2 on Si with a 300-nm SiO_2 layer at varying IR excitation energies $\hbar\omega = 0.85$–1.1 eV at room temperature. No changes are observable in the PL spectral shape. The third-order sheet susceptibility $\mathrm{Im}[\chi_S^{(3)}]$ is then obtained from the integrated

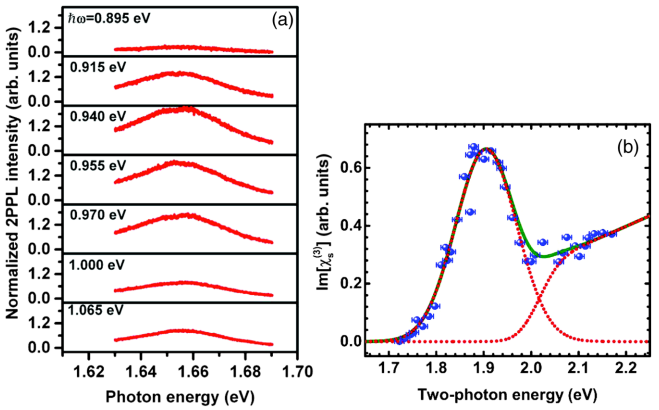

FIG. 3 (color online). (a) Representative PL spectra of monolayer WSe_2 excited by femtosecond IR pulses centered at 0.85–1.1 eV. The spectra were normalized by the SHG intensity from a z-cut single crystal quartz plate recorded under identical experimental conditions. (b) Experimental 2PPL excitation spectrum (symbols) and fit (green line) including contributions from both excitons and band-to-band transitions (dotted red lines) as described in the text.

PL intensity ($1.66 - 1.69$ eV) for each excitation energy according to Eq. (1). The result is plotted against $2\hbar\omega$ in Fig. 3(b) and for comparison also in the same plot for the linear absorption spectrum [blue symbols, Fig. 2(a)].

$\mathrm{Im}[\chi_S^{(3)}]$ shows a nonmonotonic dependence on the excitation energy with three interesting features. (i) No signal can be measured for $2\hbar\omega < 1.72$ eV. This indicates that the A exciton state is strongly suppressed, which is consistent with its assignment as a $1s$ state. (ii) $\mathrm{Im}[\chi_S^{(3)}]$ increases rapidly for $2\hbar\omega > 1.8$ eV and forms a broad peak A''. Although the limited spectral resolution and signal-to-noise ratio of this measurement does not allow us to resolve any subfeatures of the broad peak A'', a careful comparison of the two- and one-photon absorption spectrum [Fig. 2(a)] reveals consistent absorption enhancement around the energies of the $2s$, $3s$, and $4s$ states, which suggests that the broad A'' peak is likely a superposition of the corresponding np states. This assignment is consistent with the selection rules for the excitation pulse polarized in the plane of the sample [42]. On the other hand, however, it is unclear why the $2p$ state has smaller two-photon absorbance than $3p$ or $4p$. Future theoretical and experimental studies on the nature and assignment of the exciton states are warranted. (iii) $\mathrm{Im}[\chi_S^{(3)}]$ drops to a value of about half of its peak followed by a weak upward trend for $2\hbar\omega > 2$ eV. This feature is compatible with band-to-band transitions. In the simple two parabolic band model including the excitonic effect, the two-photon absorption transition rate of the band-to-band transitions scales linearly with the two-photon energy $\sim 1 + [(2\hbar\omega - E_g)/4E_b]$ when $2\hbar\omega$ is above the band gap energy E_g [42]. We describe the experimental 2PPL excitation spectrum [symbols, Fig. 3(b)] by the sum (solid green line) of a Gaussian function (dotted red line), which qualitatively accounts for the total contribution of all p states, and a linear function with a step at the band gap energy (dotted red line). A good agreement is obtained for $E_g = 2.02$ eV with a broadening of 80 meV. We thus determine the A exciton binding energy in monolayer WSe_2 to be $E_g - E_{1s} = 0.37$ eV.

Finally, we would like to understand the origin of the non-Rydberg exciton series observed in monolayer WSe_2. In the energy diagram of Fig. 4, we represent the s states by red lines at their peak energies (one-photon active) and the broad A'' state by a blue box (two-photon active). In the right panel, we compare it to the 2D hydrogenic model, in which the bottom of the continuum and the exciton binding energy have been assumed to be the same as in the experiment (2.02 and 0.37 eV, respectively). The experimental states are clearly much more evenly spaced than predicted by the 2D hydrogenic model. For instance, the $1s$ and $2s$ splitting contributes to $<1/2$ instead of the predicted $8/9$ of the total exciton binding energy [19,24]. Such a behavior can be qualitatively understood by considering the problem of dielectric screening in 2D [19]. Dielectric screening in a 2D semiconductor is significantly reduced compared to its 3D analog since the material is polarizable only in the plane. This effect explains the large level spacing and binding energies of the excitons in monolayer WSe_2. Further, as a result of the induced in-plane polarization, two-point charges living in a 2D plane interact effectively as two thin rods with charges decaying into the out-of-plane direction [19]. Thus, at large distances, the interaction behaves as an unscreened Coulomb potential, but at small distances diverges logarithmically, resulting in a weaker interaction potential. Such nonlocal screening affects the low-energy states the most (by lifting their energies) because of their small radii and results in a non-Rydberg series. We note that while a non-Rydberg series could also arise from nonparabolic band dispersion, this factor does not play any significant role in monolayer WSe_2. Both the conduction and valence bands near the

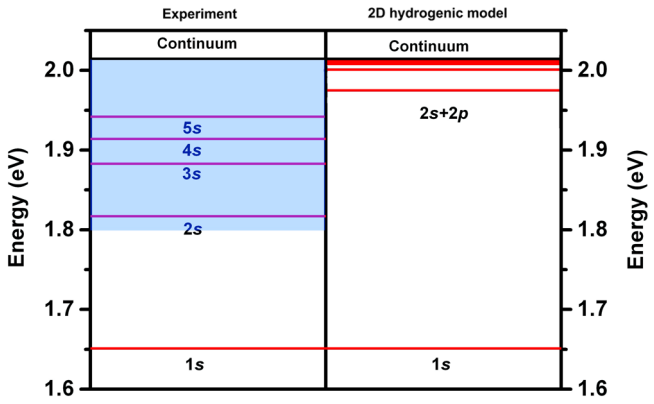

FIG. 4 (color online). Exciton excitation spectrum of monolayer WSe_2 determined experimentally in this work (left panel) is compared with the 2D hydrogenic model (right panel). Red lines denote the one-photon active states and the blue box is the unresolved two-photon active states. The exciton binding energy and the bottom of the continuum in the 2D hydrogenic model are chosen to match the values obtained from experiment.

$K(K')$ point can be well described by parabolic dispersion [9,43]. With increasing energies, the states are expected to be more Rydberg-like and provide better basis for the estimation of the exciton binding energy based on the 2D hydrogenic model. For instance, we obtain a binding energy of 0.33 eV from the 4*s* and 5*s* state, which is fully compatible with the value determined from 2PPL. (See the Supplemental Material [37], Sec. 3, for details).

In conclusion, we have directly probed, by complementary linear and nonlinear optical methods, the exciton excitation spectrum and the band gap in WSe_2 monolayers. The tightly bound excitons in this material allow us to observe up to five exciton states in linear absorption even at room temperature. The 2PPL excitation spectroscopy determines the band gap energy to be 2.02 eV, revealing a large exciton binding energy of 0.37 eV. These results are distinct from the predictions of the simple 2D hydrogenic model that ignores screening. Since optically active excitons play a central role in most optoelectronic processes, the observed large exciton binding energy and exciton excitation spectrum form a basis for future understanding and optimization of optoelectronic devices based on 2D semiconductors.

This work was supported by the Research Corporation Scialog Program and the National Science Foundation Grants No. DMR-0349201 and No. 0907477 at Case Western Reserve University and the National Science Foundation Grant No. DMR-0954486 at the University of Kansas. K. F. M. acknowledges support by the Kevli Institute at Cornell for Nanoscale Science.

[1] S. Z. Butler *et al.*, ACS Nano **7**, 2898 (2013).
[2] T. Cheiwchanchamnangij and W. R. L. Lambrecht, Phys. Rev. B **85**, 205302 (2012).
[3] A. Ramasubramaniam, Phys. Rev. B **86**, 115409 (2012).
[4] D. Y. Qiu, F. H. da Jornada, and S. G. Louie, Phys. Rev. Lett. **111**, 216805 (2013).
[5] J. Feng, X. Qian, C.-W. Huang, and J. Li, Nat. Photonics **6**, 866 (2012).
[6] F. Hüser, T. Olsen, and K. S. Thygesen, Phys. Rev. B **88**, 245309 (2013).
[7] G. Berghäuser and E. Malic, Phys. Rev. B **89**, 125309 (2014).
[8] H.-P. Komsa and A. V. Krasheninnikov, Phys. Rev. B **86**, 241201 (2012).
[9] T. C. Berkelbach, M. S. Hybertsen, and D. R. Reichman, Phys. Rev. B **88**, 045318 (2013).
[10] A. S. Rodin and A. H. Castro Neto, Phys. Rev. B **88**, 195437 (2013).
[11] K. F. Mak, C. Lee, J. Hone, J. Shan, and T. F. Heinz, Phys. Rev. Lett. **105**, 136805 (2010).
[12] A. Splendiani, L. Sun, Y. Zhang, T. Li, J. Kim, C.-Y. Chim, G. Galli, and F. Wang, Nano Lett. **10**, 1271 (2010).
[13] R. C. Miller, D. A. Kleinman, W. T. Tsang, and A. C. Gossard, Phys. Rev. B **24**, 1134 (1981).
[14] R. L. Greene, K. K. Bajaj, and D. E. Phelps, Phys. Rev. B **29**, 1807 (1984).
[15] S. M. Sze, *Semiconductor Devices: Physics and Technology* (John Wiley & Sons, New York, 2002).
[16] K. F. Mak, K. He, C. Lee, G. H. Lee, J. Hone, T. F. Heinz, and J. Shan, Nat. Mater. **12**, 207 (2013).
[17] J. S. Ross *et al.*, Nat. Commun. **4**, 1474 (2013).
[18] A. K. M. Newaz, D. Prasai, J. I. Ziegler, D. Caudel, S. Robinson, R. F. Haglund Jr, and K. I. Bolotin, Solid State Commun. **155**, 49 (2013).
[19] P. Cudazzo, I. V. Tokatly, and A. Rubio, Phys. Rev. B **84**, 085406 (2011).
[20] B. L. Evans and P. A. Young, Proc. Phys. Soc. London **91**, 475 (1967).
[21] A. R. Beal, W. Y. Liang, and J. C. Knights, J. Phys. C **5**, 3540 (1972).
[22] After submission of this work, the following experimental and theoretical studies on exciton binding energy and exciton excited states in monolayer TMDs have been reported: A. Chernikov, T. C. Berkelbach, H. M. Hill, A. Rigosi, Y. Li, O. B. Aslan, D. R. Reichman, M. S. Hybertsen, and T. F. Heinz, arXiv:1403.4270; B. Zhu, X. Chen, and X. Cui, arXiv:1403.5108; Z. Ye, T. Cao, K. O'Brien, H. Zhu, X. Yin, Y. Wang, S. G. Louie, and X. Zhang, arXiv:1403.5568; G. Wang, X. Marie, I. Gerber, T. Amand, D. Lagarde, L. Bouet, M. Vidal, A. Balocchi, and B. Urbaszek, arXiv:1404.0056; M. M. Ugeda *et al.*, arXiv:1404.2331; T. Stroucken and S. W. Koch, arXiv:1404.4238.
[23] M. C. Peter and Y. Yu, *Fundamentals of Semiconductors* (Springer, New York, 2010).
[24] X. L. Yang, S. H. Guo, F. T. Chan, K. W. Wong, and W. Y. Ching, Phys. Rev. A **43**, 1186 (1991).
[25] K. Tai, A. Mysyrowicz, R. J. Fischer, R. E. Slusher, and A. Y. Cho, Phys. Rev. Lett. **62**, 1784 (1989).
[26] F. Wang, G. Dukovic, L. E. Brus, and T. F. Heinz, Science **308**, 838 (2005).
[27] J. Maultzsch, R. Pomraenke, S. Reich, E. Chang, D. Prezzi, A. Ruini, E. Molinari, M. Strano, C. Thomsen, and C. Lienau, Phys. Rev. B **72**, 241402 (2005).
[28] D. Xiao, G.-B. Liu, W. Feng, X. Xu, and W. Yao, Phys. Rev. Lett. **108**, 196802 (2012).
[29] K. F. Mak, K. He, J. Shan, and T. F. Heinz, Nat. Nanotechnol. **7**, 494 (2012).
[30] H. Zeng, J. Dai, W. Yao, D. Xiao, and X. Cui, Nat. Nanotechnol. **7**, 490 (2012).
[31] T. Cao *et al.*, Nat. Commun. **3**, 887 (2012).
[32] G. Sallen *et al.*, Phys. Rev. B **86**, 081301(R) (2012).
[33] A. M. Jones *et al.*, Nat. Nanotechnol. **8**, 634 (2013).
[34] W. Zhao, Z. Ghorannevis, L. Chu, M. Toh, C. Kloc, P.-H. Tan, and G. Eda, ACS Nano **7**, 791 (2013).
[35] H. Zeng *et al.*, Sci. Rep. **3**, 1608 (2013).
[36] K. He, C. Poole, K. F. Mak, and J. Shan, Nano Lett. **13**, 2931 (2013).
[37] See the Supplemental Material at http://link.aps.org/supplemental/10.1103/PhysRevLett.113.026803, which includes Refs. [11,16,24,38,39].
[38] A. B. Kuzmenko, Rev. Sci. Instrum. **76**, 083108 (2005).
[39] A. Savitzky and M. J. E. Golay, Anal. Chem. **36**, 1627 (1964).
[40] X. Wei, S.-C. Hong, X. Zhuang, T. Goto, and Y. R. Shen, Phys. Rev. E **62**, 5160 (2000).
[41] N. Bloembergen and P. S. Pershan, Phys. Rev. **128**, 606 (1962).
[42] A. Shimizu, Phys. Rev. B **40**, 1403 (1989).
[43] Y. Song and H. Dery, Phys. Rev. Lett. **111**, 026601 (2013).

nature materials

LETTERS

PUBLISHED ONLINE: 31 AUGUST 2014 | DOI: 10.1038/NMAT4061

Giant bandgap renormalization and excitonic effects in a monolayer transition metal dichalcogenide semiconductor

Miguel M. Ugeda[1*†], Aaron J. Bradley[1†], Su-Fei Shi[1†], Felipe H. da Jornada[1,2], Yi Zhang[3,4], Diana Y. Qiu[1,2], Wei Ruan[1,5], Sung-Kwan Mo[3], Zahid Hussain[3], Zhi-Xun Shen[4,6], Feng Wang[1,2,7], Steven G. Louie[1,2] and Michael F. Crommie[1,2,7*]

Two-dimensional (2D) transition metal dichalcogenides (TMDs) are emerging as a new platform for exploring 2D semiconductor physics[1–9]. Reduced screening in two dimensions results in markedly enhanced electron–electron interactions, which have been predicted to generate giant bandgap renormalization and excitonic effects[10–13]. Here we present a rigorous experimental observation of extraordinarily large exciton binding energy in a 2D semiconducting TMD. We determine the single-particle electronic bandgap of single-layer $MoSe_2$ by means of scanning tunnelling spectroscopy (STS), as well as the two-particle exciton transition energy using photoluminescence (PL) spectroscopy. These yield an exciton binding energy of 0.55 eV for monolayer $MoSe_2$ on graphene—orders of magnitude larger than what is seen in conventional 3D semiconductors and significantly higher than what we see for $MoSe_2$ monolayers in more highly screening environments. This finding is corroborated by our *ab initio* GW and Bethe–Salpeter equation calculations[14,15] which include electron correlation effects. The renormalized bandgap and large exciton binding observed here will have a profound impact on electronic and optoelectronic device technologies based on single-layer semiconducting TMDs.

The remarkable properties of atomically thin semiconducting TMD layers include an indirect-to-direct bandgap crossover[1,2,9], field-induced transport with high on–off ratios[16], valley-selective circular dichroism[3–6], and a strong photovoltaic response[17,18]. Fundamental understanding of the electron/hole quasiparticle band structure and many-body interactions in 2D TMDs, however, is still lacking. Enhanced Coulomb interactions due to low-dimensional effects are expected to increase the quasiparticle bandgap as well as to cause electron–hole pairs to form more strongly bound excitons[10–13]. Such effects have been observed previously in other reduced dimensional systems, including carbon nanotubes[19] and nanostructured materials[20]. Untangling optoelectronic many-body effects in single-layer TMDs requires measurement of both the electronic bandgap and the optical bandgap, the most fundamental parameters for transport and optoelectronics applications. The electronic bandgap (E_g) characterizes single-particle (or quasiparticle) excitations and is defined by the sum of the energies needed to separately tunnel an electron and a hole into monolayer $MoSe_2$. The optical bandgap (E_{opt}) describes the energy required to create an exciton, a correlated two-particle electron–hole pair, via optical absorption. The difference in these energies (E_g–E_{opt}) directly yields the exciton binding energy (E_b) with no need for further modelling. Here we provide evidence for significant Coulomb-driven quasiparticle bandgap renormalization and unusually strong exciton stability in 2D TMDs through the independent determination of E_g and E_{opt} using STS and PL spectroscopy. Using this technique we also directly observe a reduction in exciton binding energy as substrate screening is increased.

STS and PL measurements were both carried out on the same high-quality submonolayer $MoSe_2$ films grown on epitaxial bilayer graphene (BLG) on 6H-SiC(0001) as well as on cleaved graphite (HOPG) substrates. Because the $MoSe_2$ surface coverage for our samples was typically ∼0.8 ML, we were able to simultaneously image the $MoSe_2$ monolayer and the underlying substrate using scanning tunnelling microscopy (STM). Figure 1b,d shows atomically resolved STM images taken of a $MoSe_2$ monolayer region and a BLG substrate region, respectively. The BLG substrate (Fig. 1d) shows typical hexagonal atomic contrast due to the Bernal AB stacking overlaid with the $(6\sqrt{3} \times 6\sqrt{3})$ SiC reconstruction[21]. The high-resolution STM image acquired on $MoSe_2$ (Fig. 1b) shows a honeycomb atomic lattice with one sublattice brighter than the other. Both sublattices show a unit cell of 3.3 Å, corresponding to the interatomic spacing in both the basal Se and Mo planes of $MoSe_2$ (Supplementary Information). The larger-scale $MoSe_2$/BLG image (Fig. 1c) shows only one sublattice owing to a slightly lower (and more typical) spatial resolution. The atomic registry of the $MoSe_2$ lattice was often oriented precisely with the graphene lattice (yellow arrows in Fig. 1b,d), but also frequently showed a slight rotation angle (dashed purple lines in Fig. 1c). An additional periodic superlattice was always visible in the STM images (Fig. 1b,c). This superlattice is explained by the fact that when

[1]Department of Physics, University of California at Berkeley, Berkeley, California 94720, USA, [2]Materials Sciences Division, Lawrence Berkeley National Laboratory, Berkeley, California 94720, USA, [3]Advanced Light Source, Lawrence Berkeley National Laboratory, Berkeley, California 94720, USA, [4]Stanford Institute for Materials and Energy Sciences, SLAC National Accelerator Laboratory, Menlo Park, California 94025, USA, [5]State Key Laboratory of Low Dimensional Quantum Physics, Department of Physics, Tsinghua University, Beijing 100084, China, [6]Geballe Laboratory for Advanced Materials, Departments of Physics and Applied Physics, Stanford University, Stanford, California 94305, USA, [7]Kavli Energy NanoSciences Institute at the University of California Berkeley and the Lawrence Berkeley National Laboratory, Berkeley, California 94720, USA. †These authors contributed equally to this work.
*e-mail: mmugeda@berkeley.edu; crommie@berkeley.edu

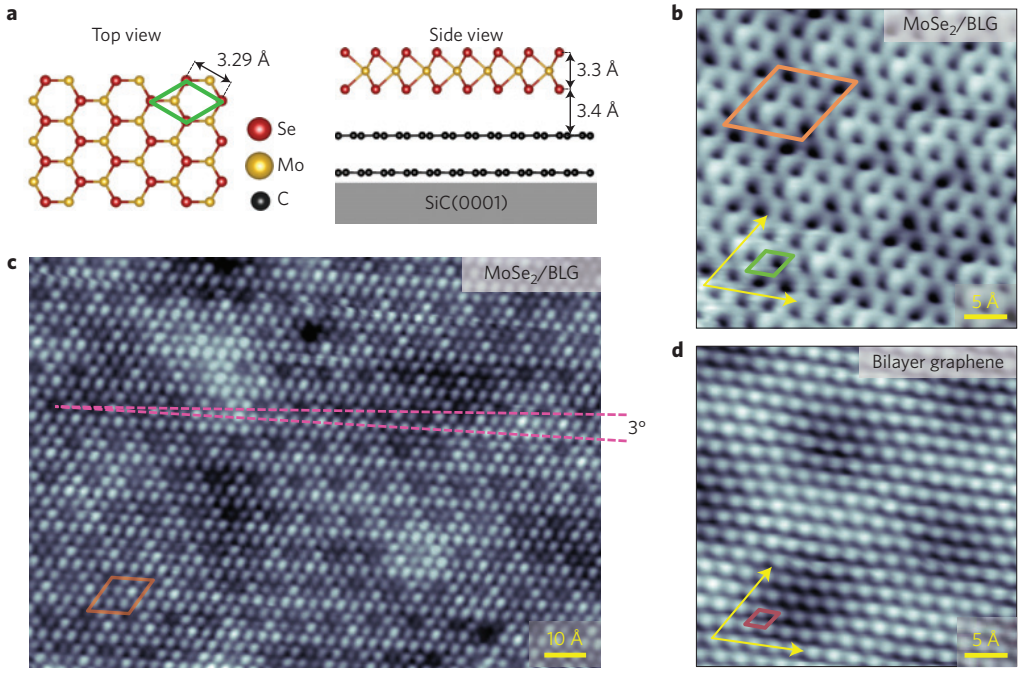

Figure 1 | Morphology of monolayer $MoSe_2$ on bilayer graphene. a, Top and side view sketches of monolayer $MoSe_2$, including the substrate. **b**, High-resolution STM image of $MoSe_2$ ($V_s = -1.53$ V, $I_t = 3$ nA, $T = 5$ K). **c**, STM image (typical resolution) of monolayer $MoSe_2$ showing a 9.7 Å × 9.7 Å moiré pattern with an angle of 3° between the moiré pattern and the $MoSe_2$ lattice ($V_s = -0.9$ V, $I_t = 20$ pA, $T = 5$ K). **d**, High-resolution STM image of BLG ($V_s = -0.5$ V, $I_t = 30$ pA, $T = 5$ K). Unreconstructed unit cells are indicated in green for $MoSe_2$ and dark red for BLG. Approximate moiré pattern unit cell for $MoSe_2$ is outlined in orange.

the $MoSe_2$ and graphene lattices are overlaid, four graphene unit cells accommodate three unit cells of $MoSe_2$, thus forming a quasicommensurate 9.87 Å × 9.87 Å superstructure (a moiré pattern) as observed in the STM images of $MoSe_2$. Rotationally misaligned $MoSe_2$ domains show slightly smaller incommensurate moiré patterns. Similar structure was seen in STM images of a single layer of $MoSe_2$ grown on HOPG (Supplementary Information).

We experimentally investigated both the electronic structure and optical transitions in monolayer $MoSe_2$ by combining STS and PL spectroscopy. Figure 2b shows a typical STM dI/dV spectrum acquired on monolayer $MoSe_2$/BLG. The observed electronic structure is dominated by a large electronic bandgap surrounded by features labelled V_{1-4} in the valence band (VB) and C_1 in the conduction band (CB). The $MoSe_2$ band edges are best determined by taking the logarithm of dI/dV, as shown in Fig. 2d. There the VB maximum (VBM) for monolayer $MoSe_2$ is seen to be located at -1.55 ± 0.03 V and the CB minimum (CBM) at 0.63 ± 0.02 V. The relative position of E_F ($V_{bias} = 0$ V) with respect to the band edges reveals n-type doping for our samples, although with a very low carrier concentration. We tentatively attribute the n-doping of our $MoSe_2$ samples to intrinsic point defects such as vacancies and/or lattice antisites, which have been found to be responsible for n-doping in similar materials[22]. Our STS measurements yield a value for the single-particle electronic bandgap for $MoSe_2$/BLG of $E_g = E_{CBM} - E_{VBM} = 2.18 \pm 0.04$ eV. Similar behaviour is seen for $MoSe_2$/HOPG, except that the electronic bandgap is reduced by 11% owing to the different dielectric screening properties of the two substrates (Supplementary Information). The uncertainty in E_g arises from both lateral positional variations as well as tip-induced electronic artefacts (which we broadly refer to as tip-induced band bending (TIBB); Supplementary Information). TIBB can arise owing to poor screening of electric fields at a semiconducting surface[23]. We are able to rule out TIBB as a significant source of error in our E_g measurements by two methods: tip–sample distance variation (which allows us to access different electric field values) and comparison of our spectra with our angle-resolved photoemission spectroscopy (ARPES). In this comparison, we find that the V_1 feature, for example, arises from the spin–split valence band at the K-point that is seen for single-layer semiconducting TMDs (see Supplementary Information for a more detailed STS/ARPES comparison).

Measurement of the optical bandgap (E_{opt})—that is, the electron–hole excitation energy—was performed using PL spectroscopy. PL from single-layer $MoSe_2$ on either graphene or HOPG is strongly quenched by non-radiative channels opened by the substrate, but the PL signal is still clearly observable as a well-defined peak. A representative set of data taken at two different temperatures for $MoSe_2$/BLG is shown in Fig. 3. At room temperature, the PL spectra show a clear Lorentzian shape centred at 1.55 ± 0.01 eV. At 77 K, the peak position of the PL is shifted to 1.63 ± 0.01 eV. This decrease of photon energy at high temperature has been observed previously[24] and is attributed to thermal reduction of the $MoSe_2$ electronic bandgap. As previous studies[24] have shown that PL does not shift significantly when the temperature drops below 77 K, we determine the low-temperature $MoSe_2$/BLG optical bandgap to be $E_{opt} = 1.63 \pm 0.01$ eV (uncertainty here arises from spatial variations and temperature dependence). The optical bandgap rises only slightly (by 2%) for $MoSe_2$/HOPG (Supplementary Information).

The $MoSe_2$/BLG optical bandgap of $E_{opt} = 1.63$ eV differs from the electronic bandgap $E_g = 2.18$ eV by the amount 0.55 ± 0.04 eV, which corresponds to the binding energy of the $MoSe_2$/BLG electron–hole excitation. For $MoSe_2$/HOPG we find that the exciton binding energy is reduced by 51% compared to $MoSe_2$/BLG, which shows directly how increased environmental screening reduces this quantity. The exciton binding energy seen for single-layer $MoSe_2$/BLG is two orders of magnitude higher than the binding energy seen in conventional semiconductors such as Si or Ge.

To better understand and interpret our experimental findings, we performed *ab initio* GW (ref. 14) and GW plus Bethe–Salpeter equation (GW–BSE) calculations[15,25] on $MoSe_2$

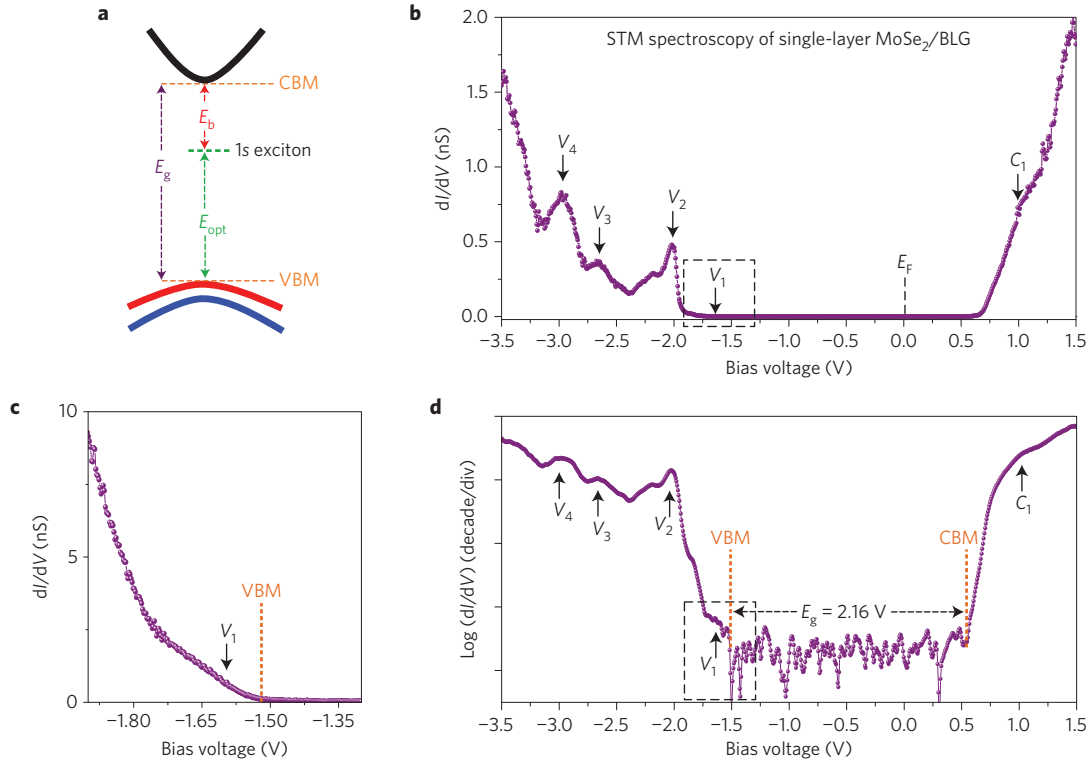

Figure 2 | Electronic structure of monolayer $MoSe_2$ on bilayer graphene. a, Energy diagram schematically indicating the electronic bandgap (E_g), the optical bandgap (E_{opt}), and the exciton binding energy (E_b). **b**, STM dI/dV spectrum acquired on monolayer $MoSe_2$/BLG showing the electronic bandgap and nearby electronic features: V_{1-4} in the valence band (VB) and C_1 in the conduction band (CB) ($f = 873$ Hz, $I_t = 5$ nA, $V_{rms} = 3$ mV, $T = 5$ K). **c**, Close-up view of $MoSe_2$ STS (boxed region in **b** and **d**) showing the valence band maximum (VBM) and V_1 feature ($f = 873$ Hz, $I_t = 4$ nA , $V_{rms} = 2$ mV, $T = 5$ K). **d**, Logarithm of a typical dI/dV spectrum used in the statistical analysis to obtain E_g ($f = 873$ Hz, $I_t = 5$ nA, $V_{rms} = 3$ mV, $T = 5$ K).

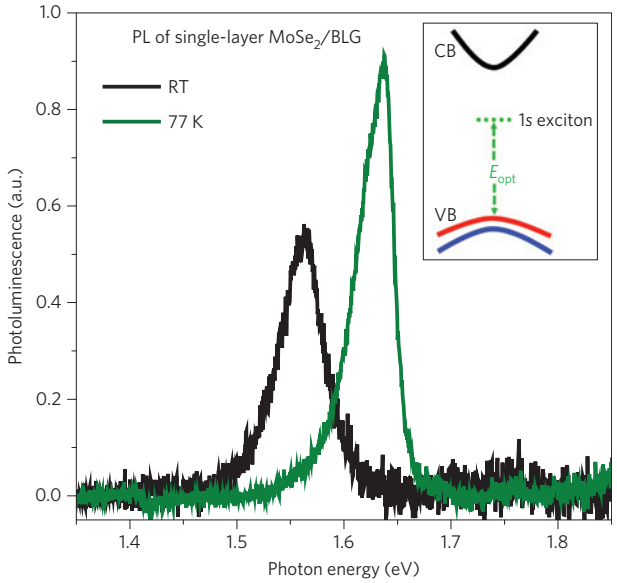

Figure 3 | Optical characterization of monolayer $MoSe_2$ on bilayer graphene. Representative photoluminescence spectra acquired at room temperature (RT; black) and at 77 K (green) for 0.8 ML $MoSe_2$ on a BLG/SiC substrate. The photoluminescence at room temperature is centred at 1.55 eV. The peak shifts to 1.63 eV at 77 K. This photoluminescence peak corresponds to the lowest-energy exciton transition (E_{opt}) in single-layer $MoSe_2$ (inset).

using the BerkeleyGW package[25]. This allowed computation of the monolayer $MoSe_2$/BLG quasiparticle structure and optical transitions, including electron–hole interactions. (For details of the calculations, see Supplementary Information). Within this approach we found that $MoSe_2$ monolayers are direct gap semiconductors at both the DFT and GW levels of theory. For quantitative comparison between experiment and theory we had to take into account the screening of the $MoSe_2$ layer by the BLG underneath (the screening from SiC was neglected because its polarizability is much smaller than that of BLG). Substrate screening is expected to decrease both the quasiparticle bandgap and the exciton binding energy of an isolated $MoSe_2$ layer. To avoid the high computational demands of performing a highly converged calculation for the explicit $MoSe_2$/BLG supercell system, we developed a novel method to incorporate substrate screening. We first separated the total screening into the intrinsic $MoSe_2$ and the BLG substrate contributions[26]. We calculated within the random phase approximation (RPA) the intrinsic contribution of $MoSe_2$ fully from first principles, including all local field effects. For the substrate contribution, we fully took into account the in-plane substrate long-wavelength screening and the full perpendicular component of the screening while neglecting in-plane local fields produced by the substrate (this is justified by the in-plane delocalization of the π orbitals in graphene). Within this approach we calculated a quasiparticle bandgap of 2.13 ± 0.10 eV for $MoSe_2$/BLG, in good agreement with the experimental value of 2.18 ± 0.04 eV. The theoretical uncertainty arises primarily as a result of the GW approximation of the electronic self-energy (Supplementary Information).

Combining this screening approach with the GW–BSE method allowed us to calculate the optical spectrum and the exciton binding energy of a $MoSe_2$ monolayer both with and without BLG substrate screening. We find that the BLG substrate decreases the exciton binding energy from 0.65 ± 0.10 eV to 0.52 ± 0.10 eV, with the latter value in good agreement with the corresponding experimental

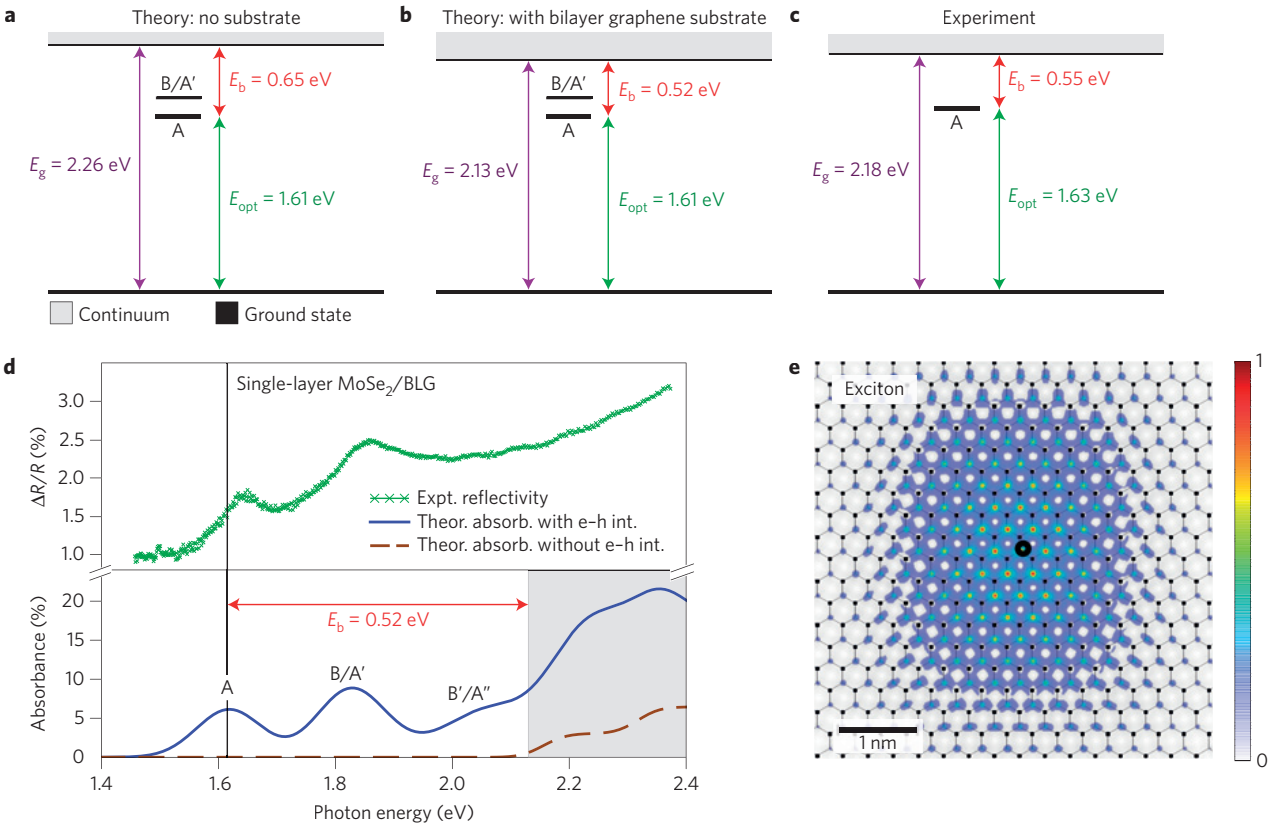

Figure 4 | Comparison between *ab initio* excited-state calculations and single-layer $MoSe_2$ experiment. a–c, Relevant energy levels sketched for GW-BSE calculation without substrate (**a**), GW-BSE calculation with BLG substrate (**b**) and experimental data (**c**). **d**, Calculated optical absorbance of single-layer $MoSe_2$ with and without electron–hole interactions, including BLG screening. A constant Gaussian broadening of $\sigma = 50$ meV (30 meV) was used in the curve with (without) electron–hole interactions. The shaded grey area corresponds to energies above the single-particle electronic gap. The experimental differential reflectivity spectrum measured at 77 K is shown in green. **e**, Spatial map of the exciton wavefunction corresponding to the excitonic peak labelled A in **a–d** (wavefunction is shown with the hole (black circle) fixed in space). Mo atoms are small black squares, Se atoms not shown.

$MoSe_2$/BLG value of 0.55 ± 0.04 eV. Similarly, the calculated optical gap for $MoSe_2$/BLG is found to be 1.61 ± 0.14 eV, in good agreement with the measured optical gap of 1.63 ± 0.01 eV. The calculated electronic bandgap, optical gap and exciton binding energies are all graphically compared with the experimental results in the energy level diagrams of Fig. 4a–c. In Fig. 4d, we compare our calculated optical absorption spectrum with experimental reflectivity data for $MoSe_2$/BLG. We observe good agreement between experiment and theory for the first two excitonic peaks (A and B). Higher-energy excitonic states, such as A′ and B′, are known to be more affected by electron–phonon interactions[13] (not included in the present calculation) and are more spectrally broadened. Figure 4e shows the predicted spatial dependence of the lowest-energy bright exciton state.

Our theoretical and experimental results reveal that many-electron interactions are strong in $MoSe_2$/BLG and prominently affect the quasiparticle excitations and optical response of this system. The 51% reduction seen for the exciton binding energy in $MoSe_2$/HOPG arises from the stronger substrate screening, which reduces both the quasiparticle electronic gap and the exciton binding energy without significantly changing the optical gap. Our results directly demonstrate that increased free-carrier screening in graphite plays a large role in determining the TMD exciton binding energy[27,28]. Similar behaviour on the quasiparticle electronic gap has indeed been observed in previous ARPES measurements on highly doped $MoSe_2$ (ref. 9). The strong, environmentally dependent, exciton binding energies observed here should play a significant role in the room-temperature performance of optoelectronic nanodevices composed of single-layer semiconducting TMDs as well as more complex layered heterostructures.

Methods

The measurements were carried out on high-quality submonolayer $MoSe_2$ films grown by molecular beam epitaxy on epitaxial BLG on 6H-SiC(0001), as well as on HOPG substrates. The structural quality of the samples and the $MoSe_2$ coverage were characterized by *in-situ* reflection high-energy electron diffraction (RHEED), low-energy electron diffraction (LEED), core-level spectroscopy, and Raman spectroscopy (Supplementary Information). STM imaging and STS experiments were performed in an ultrahigh vacuum (UHV) system equipped with a home-built scanning tunnelling microscope operated at $T = 5$ K. STM differential conductance (dI/dV) spectra were measured at 5 K using standard lock-in techniques. To avoid tip artefacts, the STM tip was calibrated by measuring reference spectra on the graphene substrate[29,30] (Supplementary Information). PL experiments were performed in high vacuum using continuous wave excitation centred at 532 nm with a power of 500 μW and a focused spot size of 2 μm. Different spots across the sample consistently showed similar PL, absorption and STS spectra. Differential reflection spectra were taken using a supercontinuum laser (~470–1,800 nm) focused to a spot size of 2 μm. Both STM/STS and optical measurements were performed consecutively on the same samples.

Received 24 March 2014; accepted 16 July 2014; published online 31 August 2014

References

1. Mak, K. F. *et al.* Atomically thin MoS_2: A new direct-gap semiconductor. *Phys. Rev. Lett.* **105,** 136805 (2010).

2. Splendiani, A. *et al.* Emerging photoluminescence in monolayer MoS_2. *Nano Lett.* **10,** 1271–1275 (2010).
3. Mak, K. F., He, K. L., Shan, J. & Heinz, T. F. Control of valley polarization in monolayer MoS_2 by optical helicity. *Nature Nanotech.* **7,** 494–498 (2012).
4. Zeng, H. L. *et al.* Valley polarization in MoS_2 monolayers by optical pumping. *Nature Nanotech.* **7,** 490–493 (2012).
5. Cao, T. *et al.* Valley-selective circular dichroism of monolayer molybdenum disulphide. *Nature Commun.* **3,** 1882 (2012).
6. Jones, A. M. *et al.* Optical generation of excitonic valley coherence in monolayer WSe_2. *Nature Nanotech.* **8,** 634–638 (2013).
7. Britnell, L. *et al.* Strong light–matter interactions in heterostructures of atomically thin films. *Science* **340,** 1311–1314 (2013).
8. Mak, K. F. *et al.* Tightly bound trions in monolayer MoS_2. *Nature Mater.* **12,** 207–211 (2013).
9. Zhang, Y. *et al.* Direct observation of the transition from indirect to direct band gap in atomically-thin epitaxial $MoSe_2$. *Nature Nanotech.* **9,** 111–115 (2014).
10. Cheiwchanchamnangij, T. & Lambrecht, W. R. L. Quasiparticle band structure calculation of monolayer, bilayer, and bulk MoS_2. *Phys. Rev. B* **85,** 205302 (2012).
11. Ramasubramaniam, A. Large excitonic effects in monolayers of molybdenum and tungsten dichalcogenides. *Phys. Rev. B* **86,** 115409 (2012).
12. Komsa, H. P. & Krasheninnikov, A. V. Effects of confinement and environment on the electronic structure and exciton binding energy of MoS_2 from first principles. *Phys. Rev. B* **86,** 241201 (2012).
13. Qiu, D. Y., da Jornada, F. H. & Louie, S. G. Optical spectrum of MoS_2: Many-body effects and diversity of exciton states. *Phys. Rev. Lett.* **111,** 216805 (2013).
14. Hybertsen, M. S. & Louie, S. G. Electron correlation in semiconductors and insulators: band-gaps and quasi-particle energies. *Phys. Rev. B* **34,** 5390–5413 (1986).
15. Rohlfing, M. & Louie, S. G. Electron–hole excitations and optical spectra from first principles. *Phys. Rev. B* **62,** 4927–4944 (2000).
16. Radisavljevic, B., Radenovic, A., Brivio, J., Giacometti, V. & Kis, A. Single-layer MoS_2 transistors. *Nature Nanotech.* **6,** 147–150 (2011).
17. Bernardi, M., Palummo, M. & Grossman, J. C. Extraordinary sunlight absorption and one nanometer thick photovoltaics using two-dimensional monolayer materials. *Nano Lett.* **13,** 3664–3670 (2013).
18. Gutierrez, H. R. *et al.* Extraordinary room-temperature photoluminescence in triangular WS2 monolayers. *Nano Lett.* **13,** 3447–3454 (2013).
19. Wang, F., Dukovic, G., Brus, L. E. & Heinz, T. F. The optical resonances in carbon nanotubes arise from excitons. *Science* **308,** 838–841 (2005).
20. Scholes, G. D. & Rumbles, G. Excitons in nanoscale systems. *Nature Mater.* **5,** 683–696 (2006).
21. Mallet, P. *et al.* Electron states of mono- and bilayer graphene on SiC probed by scanning-tunneling microscopy. *Phys. Rev. B* **76,** 041403 (2007).
22. Hor, Y. S. *et al.* p-type Bi_2Se_3 for topological insulator and low-temperature thermoelectric applications. *Phys. Rev. B* **79,** 195208 (2009).
23. Feenstra, R. M. & Stroscio, J. A. Tunneling spectroscopy of the GaAs(110) surface. *J. Vac. Sci. Technol. B* **5,** 923–929 (1987).
24. Ross, J. S. *et al.* Electrical control of neutral and charged excitons in a monolayer semiconductor. *Nature Commun.* **4,** 2498 (2013).
25. Deslippe, J. *et al.* BerkeleyGW: A massively parallel computer package for the calculation of the quasiparticle and optical properties of materials and nanostructures. *Comput. Phys. Commun.* **183,** 1269–1289 (2012).
26. Lischner, J., Vigil-Fowler, D. & Louie, S. G. Physical origin of satellites in photoemission of doped graphene: An *ab Initio* GW plus cumulant study. *Phys. Rev. Lett.* **110,** 146801 (2013).
27. Helveg, S. *et al.* Atomic-scale structure of single-layer MoS_2 nanoclusters. *Phys. Rev. Lett.* **84,** 951–954 (2000).
28. Zhang, C. *et al.* Direct imaging of band profile in single layer MoS_2 on graphite: Quasiparticle energy gap, metallic edge states, and edge band bending. *Nano Lett.* **14,** 2443–2447 (2014).
29. Brar, V. W. *et al.* Scanning tunneling spectroscopy of inhomogeneous electronic structure in monolayer and bilayer graphene on SiC. *Appl. Phys. Lett.* **91,** 122102 (2007).
30. Mallet, P. *et al.* Role of pseudospin in quasiparticle interferences in epitaxial graphene probed by high-resolution scanning tunneling microscopy. *Phys. Rev. B* **86,** 045444 (2012).
31. Horcas, I. *et al.* WSXM: A software for scanning probe microscopy and a tool for nanotechnology. *Rev. Sci. Instrum.* **78,** 013705 (2007).

Acknowledgements

Research supported by Office of Basic Energy Sciences, Department of Energy Early Career Award No. DE-SC0003949 (optical measurements), and by the sp^2 Program (STM instrumentation development and operation), the Theory Program (GW–BSE calculations), and the SciDAC Program on Excited State Phenomena in Energy Materials (algorithms and codes) which are funded by the US Department of Energy, Office of Basic Energy Sciences and of Advanced Scientific Computing Research, under Contract No. DE-AC02-05CH11231. Support also provided by National Science Foundation award no. 1235361 (image analysis) and National Science Foundation award no. DMR10-1006184 (substrate screening theory and calculations). Computational resources have been provided by the NSF through XSEDE resources at NICS and DOE at NERSC. A.J.B. was supported by the Department of Defense (DoD) through the National Defense Science & Engineering Graduate Fellowship (NDSEG) Program. W. R acknowledges support from the Chinese Scholarship Council (No. 201306210202). D.Y.Q. acknowledges support from NSF Graduate Research Fellowship Grant No. DGE 1106400 and S.G.L. acknowledges support of a Simons Foundation Fellowship in Theoretical Physics. STM/STS data were analysed and rendered using WSxM software[31]. S-F.S. and F.W. acknowledge X. Hong and J. Kim for technical help.

Author contributions

M.M.U., A.J.B., S-F.S., F.W. and M.F.C. conceived the work and designed the research strategy. M.M.U. and A.J.B. measured and analysed the STM/STS data in collaboration with W.R. for the $MoSe_2$/HOPG experiments. S-F.S. carried out the photoluminescence and Raman experiments. F.H.d.J. and D.Y.Q. performed the theoretical calculations. Y.Z. and S-K.M. performed the MBE growth and characterization (LEED, RHEED, core-level spectroscopy) of the samples. Z.H. and Z-X.S. supervised the MBE and sample characterization. F.W. supervised the optical measurements. S.G.L. supervised the theoretical calculations. M.F.C. supervised the STM/STS experiments. M.M.U. wrote the paper with help from A.J.B. and M.F.C. M.M.U. and M.F.C. coordinated the collaboration. All authors contributed to the scientific discussion and manuscript revisions.

Additional information

Supplementary information is available in the online version of the paper. Reprints and permissions information is available online at www.nature.com/reprints. Correspondence and requests for materials should be addressed to M.M.U. or M.F.C.

Competing financial interests

The authors declare no competing financial interests.